Improvement in Photovoltage and Stability of Porous n-Si Electrodes Coated with Platinum by Regulation of the Thickness of Nanoporous Layers

Kazuyuki Kawakami, Takashi Fujii, Shinji Yae, and Yoshihiro Nakato*

Department of Chemistry, Graduate School of Engineering Science, and Research Center for Photoenergetics of Organic Materials, Osaka University, 1-3 Machikaneyama, Toyonaka, Osaka 560, Japan

Received: November 8, 1996; In Final Form: February 11, 1997[⊗]

Porous n-Si electrodes, prepared by photoetching in HF under appropriate conditions, have macroporous layers at the surface, consisting of micrometer-sized pores and Si pillars. The wall and top of the Si pillars are further covered with 0.2−0.5-μm-thick nanoporous layers having nanometer-sized pores. The nanoporous layer can be thinned by immersion in HF. The solar cell characteristics (open-circuit photovoltage V_{OC}, fill factor, and stability) for the porous n-Si electrodes with Pt coating in 8.6 M HBr/0.05 M Br_2 were improved by thinning the nanoporous layer to an appropriate thickness, although the electrodes with no nanoporous layers gave only poor characteristics. The maximum solar energy conversion efficiency of 14% (V_{OC} 0.575 V, j_{SC} 34.7 mA·cm^{-2}, and fill factor 0.701) was obtained, which is one of the highest for n-Si photoelectrochemical solar cells. A mechanism for the generation of high V_{OC}'s as well as high fill factors in porous Si-based photoelectrochemical solar cells is discussed including a possibility of a low resistivity of the nanoporous layer for hole transport.

Introduction

Porous silicon (Si) has recently attracted much attention as a promising material for light-emitting diodes (LEDs) because it exhibits photo- and electroluminescences efficiently in the visible region.[1−5] Solar cells are closely related with LEDs, operating by a reverse mechanism to each other with respect to conversion between light and electric energies. For achieving high performances in such devices, it is important to clarify the structure and properties of porous Si layers and find a way to control them.

Considerable studies have been made on solar cells using porous Si. For p−n junction based solid-state solar cells,[6−10] porous Si is used mainly for a decrease in the surface light reflectance and an increase in the photocurrent density. For photoelectrochemical (PEC) solar cells,[11−17] the situation is rather complicated, a variety of photocurrents, photovoltages, and stabilities being reported probably because of differences in the detailed structure of porous (or nanoporous) Si layers. Some beneficial effects of using porous Si on the photovoltage were reported for hydrogen evolution on Pt-deposited p-Si,[11] photooxidation reaction on n-Si in 57% HI,[13,14] and photoreduction reaction on p-Si in nonaqueous electrolyte containing a cobaltocene/cobaltocinium redox couple,[15] and the role of porous Si in suppressing surface recombination and stabilizing the Si electrode was discussed.[14,15]

We reported before[16] that the V_{OC} for Pt-coated n-Si electrodes was increased by making a porous Si layer and explained the result by a new effect of nanometer-sized Pt−dot contacts. The purpose of the present paper is to investigate in detail the structure and properties of the Pt-coated porous n-Si electrodes on the basis of our recent advanced knowledge on the porous Si layers and the metal−dot contacts[17−20] and to search for factors to improve the characteristics.

Experimental Section

Single-crystal n-Si wafers (Shin-Etsu Handotai Co., Ltd., CZ, <100>, 0.95−1.05 Ω·cm) were cut into pieces 1 × 1 cm^2 in area, washed with boiling acetone and water, and etched with CP-4A (a mixture of hydrofluoric acid, nitric acid, acetic acid, and water (3:5:3:22 in volume)) and 12% HF. Ohmic contacts were made on the rear side with indium−gallium alloy. The n-Si piece was then placed in a Teflon holder (effective area 0.5 cm^2) and used as an n-Si electrode for the formation of a porous Si layer.

The porous Si layer was formed as follows: The n-Si electrode was illuminated (and etched) under an anodic bias in a mixture of water, 50% HF, and ethanol (21:3:4 in volume) or a mixture of 50% HF and ethanol (6:1 in volume). The n-Si surface was kept horizontal, with the etching cell placed in an ultrasonic bath (38 kHz), so that gas bubbles formed on the Si surface during the etching could easily be removed. The temperature of the cell solution was kept constant within ±1 °C using a temperature controller. A 300 W tungsten-halogen lamp was used as the light source. Currents vs potential were measured with a commercial potentiostat/galvanostat and potential programmer. After photoetching was stopped, the n-Si electrodes were in many cases kept in the above mentioned water−HF−ethanol solution at the same temperature as in the photoetching for 10−300 s without ultrasonic agitation in order to decrease the amount of the nanoporous layers.

Platinum was deposited on the n-Si wafer thus treated by the electron-beam evaporation method. The n-Si surface was inclined to the direction of the Pt vapor such that its incident angle was 75°. The Pt thickness was monitored with a quartz-oscillator placed perpendicular to the direction of the Pt vapor and regulated to be 7.0 nm as measured with this oscillator.

The Pt-deposited porous n-Si wafer was again fixed to a Teflon holder and used for measurements of solar cell characteristics. A large-area Pt plate was used as the counterelectrode, and a 8.6 M hydrogen bromide (HBr) and 0.05 M bromine (Br_2) aqueous solution was used as the redox electrolyte. The n-Si electrode was irradiated with simulated solar AM 1.5G (100 mW·cm^{-2}) light using a solar simulator (Wacom WXS-85H). The redox solution was stirred magnetically and kept at a temperature of 25 ± 1 °C during measurements.

The photoluminescence of porous n-Si layers was measured with a fluorescence spectrophotometer (Hitachi F4500). The

* Author to whom correspondence should be addressed. E-mail: nakato@chem.es.osaka-u.ac.jp. Fax: +81-6-850-6236.

[⊗] Abstract published in *Advance ACS Abstracts,* May 15, 1997.

S1089-5647(96)03742-X CCC: $14.00

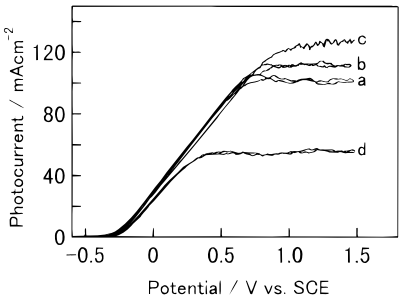

Figure 1. Photoetching currents vs potential for n-Si in water, 50% HF, and ethanol (21:3:4 in volume). The illumination intensity in mW·cm^{-2} and the cell temperature in °C are (a) 180, 30, (b) 180, 40, (c) 180, 50, and (d) 80, 50, respectively.

structure of the porous layers was inspected with a high-resolution scanning electron microscope (Hitachi S-5000). Energy dispersive X-ray spectroscopic (EDX) analysis was carried out with a Horiba EMAX-2770 spectrometer. Photocurrent action spectra were obtained using a monochromator (Jobin Yvon H20) and a 300 W Xe lamp. The intensity of monochromatic light was corrected with a radiometer/photometer (EG&G Electro-Optics 550-1) and a thermopile (Eppley).

Results

1. Structure of Porous Si Layers. Figure 1 shows photoetching currents vs potential for the formation of porous Si layers on n-Si electrodes in the water−HF−ethanol solution. The saturated photocurrent increases with the cell temperature as well as the illumination intensity. The temperature dependence may suggest that the saturated photocurrent arises from a certain diffusion-limited process such as diffusion of HF or dissolved products through fine pores formed. In the present work, the porous Si layers were formed at photocurrents much lower than the saturated photocurrent.

Figure 2 shows scanning electron micrographs (SEMs) for a porous n-Si electrode prepared by photoetching at 50 mA·cm^{-2} under 180 mW·cm^{-2} illumination at 50 °C for 5 min. The electrode surface has pores and Si pillars of a few micrometers (Figure 2A,B). The side walls of the Si pillars are covered with a spongelike layer ca. 0.2 μm thick (white layer with down in Figure 2B). The spongelike layer is also present on the top of the Si pillars in an extended form (Figure 2B). The amount of this layer on the top increased very much, forming a thick continuous layer, when the photoetching was performed at a low temperature, say, 30 °C, similar to the reports by Lévy-Clément et al.[2,21−23] The spongelike layer can be assigned to a nanoporous layer having nanometer-sized pores, as explained later.

Figure 2A also shows white parts here and there on the spongelike layer (part indicated by an arrow). These parts are assigned to Pt-deposited parts as confirmed by EDX analyses. It is to be noted that Pt was vacuum-deposited with the n-Si surface inclined to the direction of the Pt vapor (the incident angle 75°), and thus Pt was deposited mainly on one side of the spongelike layer.

Figures 3 and 4 show SEMs of n-Si electrodes that were prepared under the same conditions as Figure 2 but, after the photoetching, immersed in the water−HF−ethanol solution in the dark at the same temperature as for the photoetching (50 °C) for 40 and 300 s, respectively. The spongelike layer becomes thinner as the immersion time gets longer. The difference in the size and height of the micrometer-sized Si pillars between Figures 3 and 4 is merely due to a difference in the inspected part of the electrode. The size and height of the micrometer-sized Si pillars are nearly unchanged by this immersion. The white parts in Figure 3A and 4A are Pt-deposited parts, similar to Figure 2A.

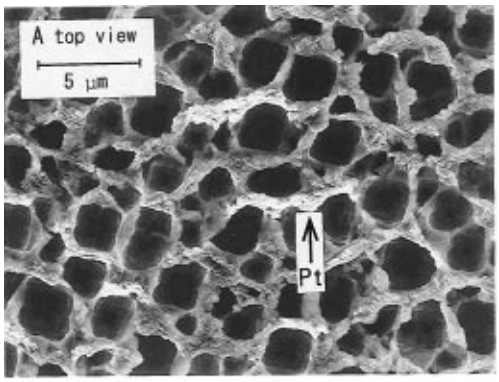

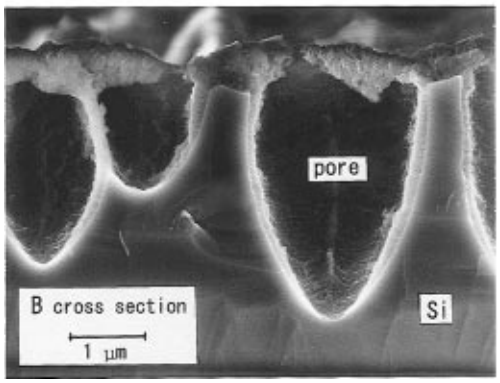

Figure 2. SEMs for a porous n-Si electrode prepared by photoetching at 50 mA·cm^{-2} under 180 mW·cm^{-2} illumination at 50 °C for 5 min and coated with Pt. The arrow shows the Pt-deposited part.

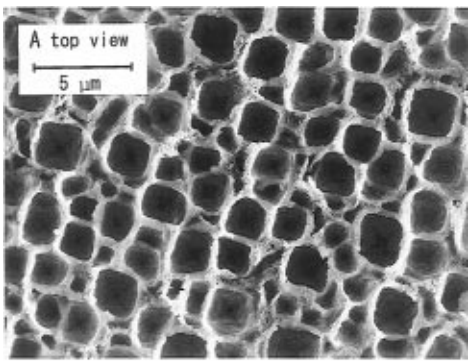

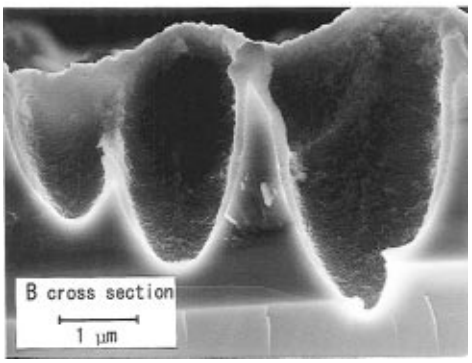

Figure 3. Same as Figure 2 except that the n-Si electrode was immersed in the water−HF−ethanol solution at 50 °C for 40 s after the photoetching was stopped.

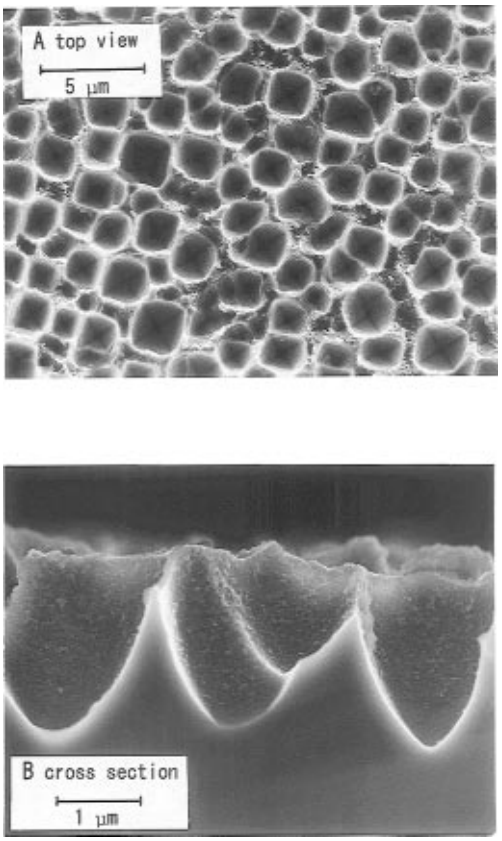

Figure 4. Same as Figures 2 and 3 except that the n-Si electrode was immersed in the water−HF−ethanol solution at 50 °C for 300 s after the photoetching was stopped.

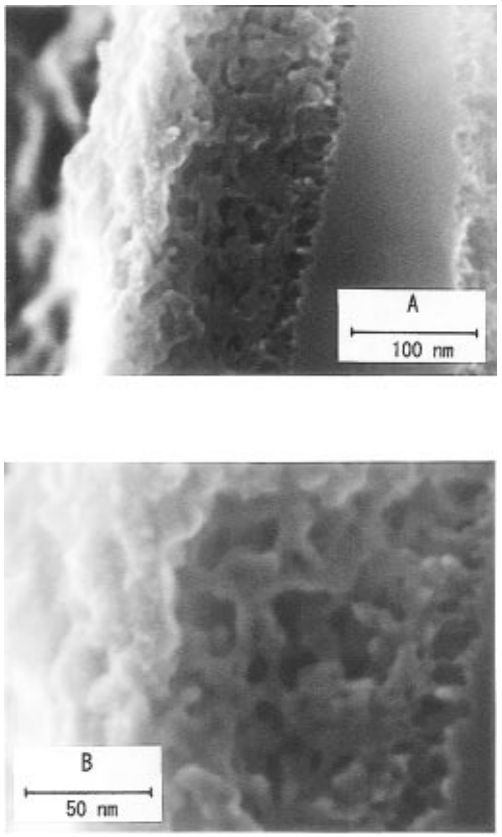

Figure 5. Cross-sectional SEMs of the spongelike (nanoporous) layer for the Figure 3-type electrode at high magnifications.

Figure 5A shows a cross-sectional SEM of the spongelike layer on the side wall of the micrometer-sized Si pillar at a high magnification, and Figure 5B does the same at a higher magnification. We can see that the layer has nanometer-sized pores and Si nets, like a nest of ants. Similar structure was reported from TEM inspection.[24−26] In the white parts of the left side of Figure 5A,B, Pt is deposited. Pt is present in a relatively extended form.

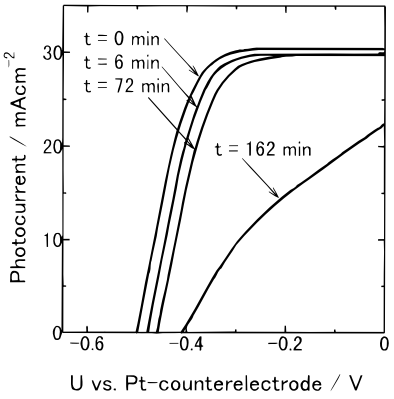

Figure 6. Stability test of the $j-U$ curve for the Figure 3-type n-Si electrode with 1.8-nm-thick Pt in 8.6 M HBr/0.05 M Br_2. The electrode was continuously illuminated at −0.2 V vs counterelectrode except when the $j-U$ curves were measured intermittently. The t in the figure represents the time passed after the start of illumination.

The n-Si electrodes prepared under the same conditions as Figure 2, hereafter called Figure 2-type electrodes, showed strong photoluminescence (PL) peaked at 545 nm. The electrodes prepared in the same way as Figure 3, called Figure 3-type electrodes, also showed the PL, but the intensity was considerably weaker than the Figure 2-type. The electrodes prepared in the same way as Figure 4, Figure 4-type electrodes, showed no PL. This result is in agreement with the above conclusion that the spongelike layer in the SEMs is the nanoporous Si layer, because the intensity of PL, reported to be emitted from the nanoporous layer,[1,2,4,5,23,24,27] decreases with decreasing spongelike layer. The conclusion is also in harmony with Halimaoui's report that the nanoporous Si layer is dissolved in HF much faster than bulk Si.[2,28] It is to be noted that the above result indicates that the thickness of the nanoporous layer can be controlled by regulating the immersion time in the water−HF−ethanol solution.

When n-Si was photoetched in a mixture of 50% HF and ethanol (6:1 in volume), its surface had quite a different structure from those of Figures 2−5. The surface had many cracks 2−3 μm wide and about 5 μm deep like the bottom of a dried marsh, instead of micrometer-sized pores and spongelike layers. The surface emitted very strong PL, indicating the formation of a thick nanoporous layer. We hereafter call the electrodes of this type dried-marsh-type electrodes.

2. Solar Cell Characteristics. The photocurrents for the Figure 2-, Figure 3-, and Figure 4-type porous n-Si electrodes decayed quickly to zero in 20−30 s without Pt coating. However, they were stabilized to large extents by Pt coating. Figure 6 shows a time course of photocurrent (j) vs potential (U) for the Figure 3-type electrode with Pt in 8.6 M HBr/0.05 M Br_2. The photocurrent in a region between 0.0 and −0.3 V vs counterelectrode was kept constant for 2 h (the electricity flowing during this period of time is 220 C·cm^{-2}) though it afterward decayed to half in 30 min. The V_{OC} decreased slightly with time during the initial 2 h (Figure 6). The Figure 3-type electrodes showed only very weak (or almost no) PL after a few cyclic potential scans though the $j-U$ curves themselves were kept unchanged on this PL-intensity change.

The photocurrent for the Figure 2-type electrode was somewhat less stable, a photocurrent of 31 mA·cm^{-2} at −0.3 V

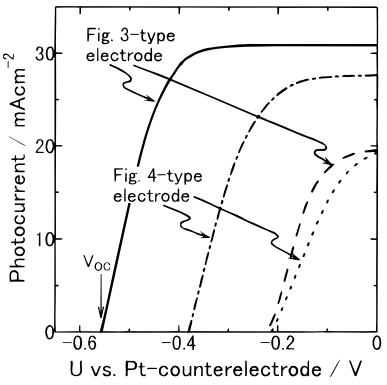

Figure 7. $j-U$ curves for the Pt-deposited Figure 3- and Figure 4-type electrodes in 8.6 M HBr/0.05 M Br_2 (solid and dot-dashed lines) and 7.6 M HI/0.05 M I_2 (dashed and dotted lines) under simulated solar illumination (AM1.5G, 100 mW·cm^{-2}).

decaying to 29 mA·cm^{-2} in ca. 80 s. This indicates that the presence of a thick spongelike (nanoporous) layer on the top of the micrometer-sized Si pillars decreases the stability. In fact, the short-circuit photocurrent j_{SC} (the photocurrent at 0.0 V) of 30 mA·cm^{-2} for an electrode having a spongelike layer much thicker than seen in Figure 2, prepared by photoetching at a low temperature, decayed to 10 mA·cm^{-2} in 2 min. On the other hand, the photocurrent for the Figure 4-type electrode was stable, more stable than that for the Figure 3-type electrode.

Figure 7 shows the $j-U$ curves for the Figure 3- and Figure 4-type electrodes coated with Pt in 8.6 M HBr/0.05 M Br_2 (solid and dot-dashed lines) and 7.6 M HI/0.05 M I_2 (dashed and dotted lines). The redox potentials for the HBr/Br_2 and HI/I_2 are 0.54 and 0.02 V vs SCE, respectively. The V_{OC}'s for both the electrodes become higher as the redox potential gets higher. Especially, the V_{OC} for the Figure 3-type electrode in HBr/Br_2 is much higher than that in HI/I_2. The difference in j_{SC} between HBr/Br_2 and HI/I_2 is due to the difference in the color (light absorption) of the solutions.

Table 1 summarizes the solar cell characteristics for various porous n-Si electrodes coated with Pt in 8.6 M HBr/0.05 M Br_2, including those for flat-surface (nonporous) n-Si electrodes. The V_{OC}'s for the Figure 2- and Figure 3-type electrodes range from 0.50 to 0.58 V and are much higher than those for the Figure 4-type electrodes (0.38−0.42 V), although the latter are still higher than for the flat-surface n-Si electrodes (0.31−0.36 V). The j_{SC}'s for the Figure 2-, Figure 3-, and Figure 4-type electrodes are similar to each other, in the range 25−38 mA·cm^{-2}, and are much higher than those for the flat n-Si electrodes (22−26 mA·cm^{-2}). This indicates that the j_{SC}'s are mainly determined by the matte-texture effect of the micrometer-sized pores. The maximum solar energy conversion efficiency of 14.0% (V_{OC} 0.575 V, j_{SC} 34.7 mA·cm^{-2}, and the fill factor 0.701) under AM1.5G, 100 mW·cm^{-2} illumination was obtained for the Figure 3-type electrode, whose surface structure is shown in Figure 3. This efficiency is one of the highest for the n-Si PEC solar cells reported so far.[29,30]

Figure 8 shows the effect of the incident angle (θ) of the Pt vapor during the vacuum deposition of Pt on the V_{OC} of the Figure 3-type electrode. The V_{OC} increases with θ, indicating the importance of oblique Pt deposition. The photocurrent action spectrum for the Pt-deposited Figure 3-type electrode was similar in spectral shape to that for the flat (nonporous) n-Si electrode except that the photocurrent efficiency for the former was higher than that for the latter. The specular reflectance of the porous n-Si electrode at an incident angle of 5° was measured to be nearly zero in wavelengths from 300 to 1300 nm.

The photocurrent for the dried-marsh-type porous n-Si electrode was not stabilized by the Pt coating. It first increased and then decreased, irrespective of the presence or absence of Pt, as reported by Koshida et al.[12] The first few potential scans gave an unusually high V_{OC} of 0.740−0.800 V, indicating that the photocurrent is arising from the electrode corrosion.

Discussion

From the results described in the preceding section, we can conclude that high V_{OC}'s and stable photocurrents are obtained for the Pt-coated Figure 3-type porous n-Si electrodes having moderately thick nanoporous layers. The electrodes having too thick nanoporous layers, such as the Figure 2-type and dried-marsh-type electrodes, generate high V_{OC}'s but are unstable even with Pt. On the other hand, the electrodes having very thin or no nanoporous layers such as the Figure 4-type electrodes give stable photocurrents, but the V_{OC} is low.

It is rather surprising that the Pt-coated Figure 3-type porous n-Si electrodes not only generate high V_{OC}'s of 0.50−0.58 V, much higher than those for the Pt-coated flat-surface (nonporous) n-Si electrodes (0.31−0.37 V), but also yield very large fill factors exceeding 0.7 (Table 1). The stable photocurrent for the present electrodes can flow only when photogenerated holes arrive at deposited Pt, as clearly indicated by the quick decay of the photocurrent for the electrodes without Pt. The naked n-Si surface is immediately oxidized in the redox solution under illumination and covered with an insulating thin Si oxide layer, and no redox reaction can be assumed to proceed at the naked Si/electrolyte interface.[29] Pt is deposited only on the top of the nanoporous layer, as clearly seen in the SEM of Figure 5. Accordingly we have to consider that the efficient $j-U$ curves arise from efficient hole transport through the nanoporous layer.

However, it is reported that the nanoporous layers in which majority carriers are depleted have high electrical resistivities of 10^5-10^7 Ω·cm.[15,25,31,32] For the present porous n-Si electrode that is in contact with the redox solution having a (relatively) high redox potential, the porous layer will be completely depleted of majority carriers, similar to a reported result for porous n-Si electrode in nonaqueous solution containing oxidized and reduced dimethylferrocene.[33] This suggests that the nanoporous layer in the present electrodes should have a high resistivity, contrary to the above mentioned conclusion. Such an apparent contradiction might be explained as follows.

A schematic cross section and a plausible energy band diagram for the Pt-deposited Figure 3-type electrode are shown in Figure 9A,B, respectively. It is first to be noted that, as mentioned above, the present porous n-Si electrode is in contact with the redox solution having a high redox potential. Therefore, holes should be injected in the nanoporous layer so that the quasi-Fermi level of the holes in the nanoporous layer will agree with the redox level of the redox couple. Such injected holes are expected to contribute to the conductivity of the nanoporous layer because it is reported that the nanoporous layer in which charge carriers are not depleted has a high enough conductivity.[32]

The above argument is supported by a little more quantitative consideration. As mentioned in the preceding section, the Figure 3-type electrodes show only very weak (or almost no) PL after the $j-U$ curve measurements, although the $j-U$ curves themselves are kept unchanged. This implies that the nanoporous layer in the present work consists of Si wires with the diameter on the order of 10 nm (see also Figure 5), a little larger than the diameter for which the quantum-size effect appears.[34] Thus we can assume that the nanoporous layer in the present work

TABLE 1: Solar Cell Characteristics for the Pt-Deposited Porous and Flat (Nonporous) n-Si Electrodes in 8.6 M HBr/0.05 M Br_2: The Lowest and Highest Values Are Indicated, with the Average and Standard Deviations in Parentheses

electrode type	no. of tested samples	V_{OC} (V)	j_{SC} (mA·cm^{-2})	F. F.[a]	ϕ^{S} [b] (%)
Figure 2-type[c]	8	0.506−0.580 (0.551 ± 0.022)	24.6−36.1 (31.3 ± 3.77)	0.299−0.657 (0.477 ± 0.098)	
Figure 3-type	30	0.503−0.580 (0.550 ± 0.013)	28.4−36.1 (31.3 ± 1.30)	0.565−0.730 (0.676 ± 0.032)	10.3−14.0 (11.7 ± 0.734)
Figure 4-type	7	0.380−0.420 (0.401 ± 0.011)	27.6−37.8 (32.4 ± 2.39)	0.530−0.726 (0.628 ± 0.045)	5.65−9.88 (8.23 ± 1.17)
flat n-Si	6	0.315−0.365 (0.337 ± 0.014)	22.3−25.8 (24.3 ± 1.30)	0.557−0.656 (0.592 ± 0.033)	4.20−5.49 (4.84 ± 0.381)

[a] Fill factor. [b] Solar energy conversion efficiency (AM1.5G, 100 mW·cm^{-2}). [c] All the values are for the first few potential scans because the characteristics degraded with time.

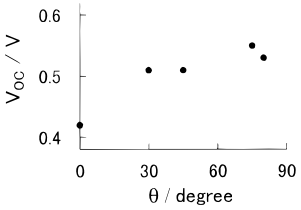

Figure 8. V_{OC} vs the incident angle (θ) of the Pt vapor during the vacuum deposition of Pt for the Figure 3-type electrode.

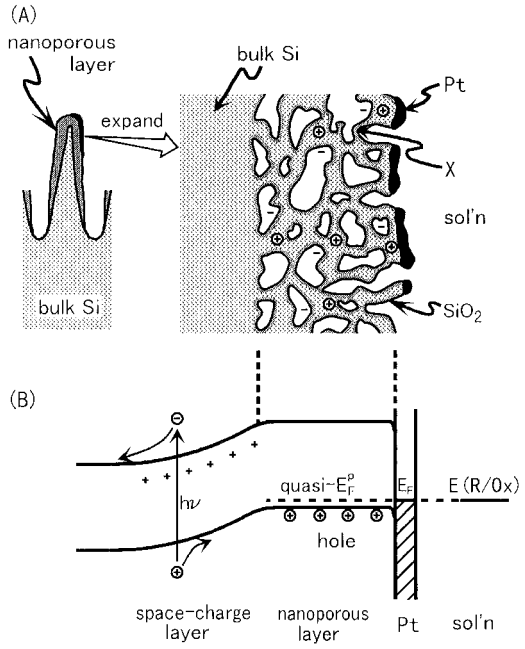

Figure 9. Schematic cross section (A) and a plausible energy band diagram (B) for the Pt-coated Figure 3-type porous n-Si electrode. E(R/Ox): the redox level of the redox couple. E_F: the Fermi level of Pt. Quasi-E_F^p: the quasi-Fermi level of holes injected by the redox couple. ⊕: hole. ⊖: electron. +: ionized donor. −: anion in solution.

has nearly the same band energies as bulk Si. The redox potential of the 8.6M HBr/0.05M Br_2 redox couple is 0.54 V vs SCE, whereas the top of the valence band at the thin-oxide-covered (Pt-free) Si surface in 8.6 M HBr without Br_2 is at about 0.3 V, as estimated from the flat-band potential of n-Si. Therefore a heavy inversion layer will be formed near the Si surface in this case, resulting in a high conductivity in the nanoporous layer. It may be noted that the width of the inversion layer is estimated to be 10 nm,[35] which is of the same order in magnitude as the diameter of the Si wires in the nanoporous layer. The 7.6 M HI/0.05 M I_2 redox couple also gives the efficient $j-U$ curve with a high fill factor (Figure 7). The redox potential of this couple is 0.02 V, and hence the quasi-Fermi level of the holes in the nanoporous layer is estimated to be about 0.3 eV above the top of the valence band. This difference of 0.3 eV corresponds to the resistivity of 200 Ω·cm, as estimated from the reported relation between the resistivity and the carrier density (impurity density) for bulk Si.[36] It then follows that the nanoporous layer of 0.5 μm thick has a resistivity on the order of 10^{-2} Ω·cm^2 and gives rise to an ohmic drop of ca. 0.3 mV for a photocurrent of 30 mA·cm^{-2}, which is negligibly small in the present work.

As an alternative explanation, we might be able to assume that a high conductivity in the nanoporous layer is achieved by a mechanism of hopping of charge carriers via surface trap sites,[25,26] because it is reported that the conductivity of the nanoporous layer by this mechanism is increased by several orders in magnitude when the layer is exposed to polar media such as ethanol and water.[34,37] It may also be advantageous that the thickness of the nanoporous layer for the present electrodes is regulated to be of moderate values, 0.1−0.5 μm, although that in the reported work in most cases ranges from 2 to 10 μm.

Now let us consider why the Pt-coated Figure 3-type porous n-Si electrodes generate high V_{OC}'s of 0.50−0.58 V. As mentioned before, the major part of the Si surface of the porous n-Si electrode is covered with thin Si-oxide, Pt being present only on top of the nanoporous layer (Figure 9A). Such a surface structure is quite similar to that for the flat-surface n-Si electrode modified with ultrafine Pt particles reported previously.[17,18] Therefore almost the same concepts can be applied to the present electrodes. According to our previous work,[17,18] three factors are important for the generation of high V_{OC}: (1) formation of a high energy barrier height, (2) efficient flow of photogenerated holes in n-Si to the solution, and (3) a very low surface carrier recombination rate.

Of these three factors, factor 2 is easily understood from the discussion made so far. Factor 3 is also understood by considering that the surface carrier recombination rate is very low at the Si/Si oxide interface and that the major part of the surface of the present electrodes is covered with Si-oxide.[17,18] The formation of a high energy barrier can be understood on the basis of the energy band diagram shown in Figure 9B. The energy barrier height for the present porous n-Si electrodes is essentially determined by the bulk Si/solution contact, not by the Si/Pt contact even when the Pt is deposited widely in the extended form. This is because the Pt/Si contact is located on top of the nanoporous layer and the modulation of the Si surface band energies by Pt is completely screened by charges within the nanoporous layer. The band bending within the Si wires in the nanoporous layer will be negligibly small if the radius of the Si wires (∼5 nm) is much less than the width of the space charge layer (∼200 nm).

The dependence of the V_{OC} on the redox couple (or the redox potential) (Figure 7) can be explained by the above argument. The higher V_{OC} for the Figure 3-type electrodes than for the Figure 4-type (Figure 7) can also be explained by the above

argument by taking into account that the Figure 3-type have moderately thick nanoporous layers whereas the Figure 4-type have only very thin or no nanoporous layers. For the latter electrodes, Pt may be deposited directly on the micrometer-sized Si pillars or on the bulk Si at the bottom of the Si pillars with a large area of Pt−Si direct contacts. Such wide-area Pt/Si contacts modulate the surface band energies of Si and hence the space charge layer in the bulk Si significantly, which leads to a large dark saturation current density (j_0) and thus low V_{OC}.[17,18]

As mentioned before, the presence of a too thick nanoporous layer decreases the electrode stability. This is also explained by the above model (Figure 9A). The nanoporous layer in the present work is expected to consist of Si nets (Si wires) having a variety of diameters. Because the thickness of the Si oxide layer formed on the Si surface is estimated, from XPS analyses for flat n-Si surface, to be 1.0−1.3 nm,[29] parts of the Si wires with a radius smaller than this value are fully oxidized and become insulating (cf. part X in Figure 9A). The amount of such parts of fine Si wires between the Pt and micrometer-sized Si pillars (bulk Si) will increase with increasing thickness of the nanoporous layer.

Figure 8 shows that the V_{OC} decreases with decreasing incident angle (θ) of the Pt vapor during the Pt deposition. This can be attributed to the fact that the nanoporous layer is very thin at the bottom of the micrometer-sized pores, as seen in Figure 3B.

The highest V_{OC} obtained for the Pt-deposited porous n-Si electrodes, 0.58 V, is still lower than the V_{OC} for flat-surface n-Si electrodes modified with colloidal Pt particles (0.61−0.63 V) reported previously.[20,38] Because the latter value is expected for the ideal, minority-carrier-controlled solar cells,[20,38] this implies that the majority-carrier dark saturation current density (j_{0n}) for the Pt-deposited Figure 3-type electrode is still not low enough. A possible reason for this is that the nanoporous Si layer may contain Si wires that are thick in the whole region between the bulk Si and Pt. This decreases the effective barrier height due to the presence of band bending within the thick Si wires and hence increases the j_{0n}. Another possible reason is that the nanoporous layer has a very large surface area (ca. 200 $m^2 \cdot cm^{-3}$),[39] and thus the probability of surface carrier recombination increases in proportion to the surface area.

In conclusion, we have studied the structure of the nanoporous Si layer in connection with the photoetching and post-treatment conditions and shown that the control of the thickness of the nanoporous Si layer is important for improving the solar cell characteristics such as the V_{OC}, the fill factor, and stability. We have also fabricated the solar cells with a high efficiency of 14.0% and discussed an operation mechanism for porous Si-based efficient and stable solar cells.

The stability problem can be solved by extending the solar cells of the present type to solid-state solar cells.[18,40,41] Also, the present method may be applied to polycrystalline Si thin films. Further studies along this line are expected to give an effective approach to high-efficiency and low-cost solar cells.

Acknowledgment. This work is partly supported by a Grant-in-Aid for Scientific Research of the Ministry of Education, Science, Sports and Culture. The authors thank Shin-Etsu Handotai Co., Ltd., for donating single-crystal n-Si wafers.

References and Notes

(1) Canham, L. T. *Appl. Phys. Lett.* **1990**, *57*, 1046.
(2) *Porous Silicon Science and Technology*; Vail, J.-C., Derrien, J., Eds.; Springer-Verlag: Berlin, Les Edirions de Physique: Les Ulis, 1995.
(3) Smith, R. L.; Collins, S. D. *J. Appl. Phys.* **1992**, *71*, R1.
(4) Searson, P. C.; Macaulay, J. M.; Prokes, S. M. *J. Electrochem. Soc.* **1992**, *139*, 3373.
(5) Jung, K. H.; Shih, S.; Kwong, D. L. *J. Electrochem. Soc.* **1993**, *140*, 3046.
(6) Prasad, A.; Balakrishnan, S.; Jain, S. K.; Jain, G. C. *J. Electrochem. Soc.* **1982**, *129*, 596.
(7) Tsuo, Y. S.; Heben, M. J.; Wu, X.; Xiao, Y.; Moore, C. A.; Verlinden, P.; Deb, S. K. *Mat. Res. Soc. Symp. Proc.* **1993**, *283*, 405.
(8) Guang-Pu, W.; Yi-Ming, Z.; Zhao-Jian, H.; Yu, L.; Jing-wei, F.; Yio-Wu, M. *Sol. Energy Mater. Sol. Cells* **1994**, *35*, 319.
(9) Sun, G.; Li, Y.; Lu, Y.; Khan, B.; Tompa, G. S. *Mat. Res. Soc. Symp. Proc.* **1995**, *358*, 593.
(10) Menna, P.; Di Francia, G.; La Ferrara, V. *Sol. Energy Mater. Sol. Cells* **1995**, *37*, 13.
(11) Koshida, N.; Echizenya, K. *J. Electrochem. Soc.* **1991**, *138*, 837.
(12) Koyama, H.; Koshida, N. *J. Electrochem. Soc.* **1991**, *138*, 254.
(13) Lévy-Clément, C.; Lagoubi, A.; Neumann-Spallart, M.; Rodot, M.; Tenne, R. *J. Electrochem. Soc.* **1991**, *138*, L69.
(14) Lévy-Clément, C.; Lagoubi, A.; Tenne, R.; Neumann-Spallart, M. *Electrochim. Acta* **1992**, *37*, 877.
(15) Mao, D.; Kim, K. J.; Tsuo, Y. S.; Frank, A. J. *J. Phys. Chem.* **1995**, *99*, 3643.
(16) Nakato, Y.; Ueda, K.; Tsubomura, H. *J. Phys. Chem.* **1986**, *90*, 5495.
(17) Nakato, Y.; Ueda, K.; Yano, H.; Tsubomura, H. *J. Phys. Chem.* **1988**, *92*, 2316.
(18) Nakato, Y.; Tsubomura, H. *Electrochim. Acta* **1992**, *37*, 897.
(19) Yae, S.; Nakanishi, I.; Nakato, Y.; Toshima, N.; Mori, H. *J. Electrochem. Soc.* **1994**, *141*, 3077.
(20) Jia, J. G.; Fujitani, M.; Yae, S.; Nakato, Y. *Electrochim. Acta* **1996**, *42*, 431.
(21) Lévy-Clément, C.; Lagoubi, A.; Tomkiewicz, M. *J. Electrochem. Soc.* **1994**, *141*, 958.
(22) Albu-Yaron, A.; Bastide, S.; Maurice, J. L.; Lévy-Clément, C. *J. Lumin.* **1993**, *57*, 67.
(23) Galun, E.; Tenne, R.; Lagoubi, A.; Lévy-Clément, C. *J. Lumin.* **1993**, *57*, 125.
(24) Albu-Yaron, A.; Bastide, S.; Bouchet, D.; Brun, N.; Colliex, C.; Lévy-Clément, C. *J. Phys. 1 Fr.* **1994**, *4*, 1181.
(25) Beale, M. I. J.; Benjamin, J. D.; Uren, M. J.; Chew, N. G.; Cullis, A. G. *J. Cryst. Growth* **1985**, *73*, 622.
(26) Lehmann, V.; Hofmann, F.; Möller, F.; Grüning, U. *Thin Solid Films* **1995**, *255*, 20.
(27) Koyama, H.; Araki, M.; Yamamoto Y.; Koshida, N. *Jpn. J. Appl. Phys.* **1991**, *30*, 3606.
(28) Halimaoui, A. *Surf. Sci. Lett.* **1994**, *306*, L550.
(29) Yae, S.; Tsuda, R.; Kai, T.; Kikuchi, K.; Uetsuji, M.; Fujii, T.; Fujitani, M.; Nakato, Y. *J. Electrochem. Soc.* **1994**, *141*, 3090.
(30) Gibbons, J. F.; Cogan, G. W.; Gronet, C. M.; Lewis, N. S. *Appl. Phys. Lett.* **1984**, *45*, 1095.
(31) Smestad, G.; Kunst, M. *Sol. Energy Mater. Sol. Cells* **1992**, *26*, 277.
(32) Anderson, R. C.; Muller, R. S.; Tobias, C. W. *J. Electrochem. Soc.* **1991**, *138*, 3406.
(33) Shen, W.-M.; Tomkiewicz, T.; Lévy-Clément, C. *J. Appl. Phys.* **1994**, *76*, 3635.
(34) Read, A. J.; Needs, R. J.; Nash, K. J.; Canham, L. T.; Calcott, P. D. J.; Qteish, A. *Phys. Rev. Lett.* **1992**, *69*, 1232.
(35) Morrison, S. R. *The Chemical Physics of Surfaces*; Plenum: New York, 1977.
(36) Sze, S. M. *Physics of Semiconductor Devices*, 2nd ed.; John Wiley & Sons: New York, 1981.
(37) Tsu, R.; Babić, D. *Appl. Phys. Lett.* **1994**, *64*, 1806.
(38) Yae, S.; Fujitani, M.; Nakanishi, I.; Uetsuji, M.; Tsuda, R.; Nakato, Y. *Sol. Energy Mater. Sol. Cells* **1996**, *43*, 311.
(39) Herino, R.; Bomchil, G.; Brala, K.; Bertrand, C.; Ginoux, J. L. *J. Electrochem. Soc.* **1987**, *134*, 1994.
(40) Nakato, Y.; Nishiura, S.; Oshika, H.; Tsubomura, H. *Jpn. J. Appl. Phys.* **1989**, *28*, L261.
(41) Nakato, Y.; Kai, K.; Kawabe, K. *Sol. Energy Mater. Sol. Cells* **1995**, *37*, 323.